

# Collective excitations in cigar-shaped spin-orbit coupled spin-1 Bose-Einstein condensates

Rajat,<sup>1,\*</sup> Arko Roy,<sup>2,3,†</sup> and Sandeep Gautam<sup>1,‡</sup>

<sup>1</sup>*Department of Physics, Indian Institute of Technology Ropar, Rupnagar-140001, Punjab, India*

<sup>2</sup>*INO-CNR BEC Center and Università di Trento, via Sommarive 14, I-38123 Trento, Italy*

<sup>3</sup>*School of Basic Sciences, Indian Institute of Technology Mandi, Mandi-175075 (H.P.), India*

We theoretically study the collective excitations of a spin-orbit-coupled spin-1 Bose-Einstein condensate with antiferromagnetic spin-exchange interactions in a cigar-shaped trapping potential at zero and finite temperatures using the Hartree-Fock-Bogoliubov theory with Popov approximation. The collective modes at zero temperature are corroborated by real-time evolution of the ground state subjected to a perturbation suitable to excite a density or a spin mode. We have also calculated a few low-lying modes analytically and found a very good agreement with the numerical results. We confirm the presence of excitations belonging to two broad categories, namely density, and spin excitations, based on the calculation of dispersion. The degeneracy between a pair of spin modes is broken by the spin-orbit coupling. At finite temperature, spin and density excitations show qualitatively different behavior as a function of temperature.

## I. INTRODUCTION

First multi-component Bose-Einstein condensate (BEC) known as spinor condensate was experimentally realized with a simultaneous optical trapping of three hyperfine-spin states from  $F = 1$  spin manifold in a gas of  $^{23}\text{Na}$  atoms [1], and was followed by the demonstration of the condensation with gas of  $^{87}\text{Rb}$  atoms in  $F = 1$  [2] and  $F = 2$  [3–5] manifolds. The vast literature on the spinor condensates covering both the experimental and theoretical progress has been reviewed in Refs. [6, 7]. One of the most important advances in the field of cold atom physics in the last decade has been an experimental demonstration of synthetic spin-orbit (SO) coupling in a pseudospin-half quantum gas [8] via light-atom interactions, which has opened up new perspectives in exploring many-body phenomena using ultracold atoms, such as topological insulators [9], the quantum anomalous Hall conductivity [10] and topological superconductors [11]. In case of spin-1 Bose-Einstein condensates (BECs), SO coupling has also been experimentally realized in a gas of  $^{87}\text{Rb}$  [12, 13] atoms by coupling three hyperfine states with Raman lasers, thus paving the way to explore the rich physics of SO-coupled spin-1 BECs. Theoretical predictions and experimental observations of SO-coupled spin-1 BECs render various novel ground-state phases including plane-wave, stripe or standing-wave, zero-momentum phases, etc. [14, 15]. Distinguishing the different phases close to the phase-transition boundaries through equilibrium density profiles is a challenge [16]. Non-equilibrium transport of spinor BECs entails various topological excitations such as solitons [17] and vortices [17, 18]. To characterize the static and dynamical properties of such systems, it is then imperative to study the collective excitations manifesting through fluctuations.

Collective modes, which are the low energy excitations of a quantum gas, can reveal fundamental information about the ultracold quantum state like the stability of different different ground state phases, fluctuations, and superfluidity,

etc. [19, 20]. To this end, it is experimentally possible to excite the low-lying dipole and breathing modes by modulating the harmonic trap and carry out spectroscopic studies with utmost precision [21]. At zero temperature, the collective excitations of the trapless pseudo-spinor and spin-1 BECs with Raman induced SO coupling have been studied theoretically [22–24] and have been found to exhibit roton-maxon structure in zero-momentum and plane-wave phases. Dynamical and energetic instabilities in the Raman-induced SO-coupled pseudospinor BEC in a uniform plane-wave phase have also been studied [25]. Experimental measurement of collective excitations through Bragg spectroscopy in Raman induced SO-coupled pseudospinor BECs, revealing the roton-maxon structure, have been carried out [26, 27]. Excitation spectrum of a one-dimensional quantum droplet for a binary mixture has been examined in Ref. [28]. However, on the contrary, theoretical studies of spinor condensates at finite temperatures are few and demand a thorough investigation. Experiments usually are performed in harmonic traps and at finite temperatures. It is therefore essential to include the effects of trapping potential and fluctuations to theoretically address such systems. It has been shown that an antiferromagnetic spin-1 Bose gas with fixed norm and magnetization undergoes double condensation using Hartree-Fock-Popov [29] and Hartree-Fock theories [30]. Phuc *et al.* [31] have studied the finite temperature phase diagram of a trapless ferromagnetic spin-1 Bose gas in the presence of quadratic Zeeman terms using Hartree-Fock-Bogoliubov theory with Popov approximation. Within the framework of Hartree-Fock theory, finite temperature phase diagram of a trapless spin-1 BEC with both linear and quadratic Zeeman terms has also been calculated [32]. Experimentally the phase diagram of an antiferromagnetic spin-1 Bose gas has been studied in Ref. [33]. Spin-mixing dynamics of a spin-1 condensate in a highly elongated trap has been studied at zero and finite temperature. [34, 35]. The effect of thermal fluctuations on the quantum phase transition from an antiferromagnetic to phase separated ground state in a spin-1 BEC has been studied in [36]. The finite temperature phase diagram of a uniform pseudospinor-half BEC with a Raman induced SO coupling shows that quantum and thermal fluctuations enlarge the phase space of a plane-wave phase [37]. A finite temperature phase transi-

\* rajat.19phz0009@iitrr.ac.in

† arko@iitmandi.ac.in

‡ sandeep@iitrr.ac.in

tion from a stripe to a plane-wave phase in a Raman induced SO-coupled pseudospinor-half  $^{87}\text{Rb}$  Bose gas has been experimentally observed [38]. A perturbation approach, valid for small Raman coupling strengths, has been used to study the transition between plane-wave and stripe phase for a Raman induced SO-coupled pseudospinor-half BEC at finite temperatures [39]. Stability of the plane-wave phase in Rashba SO-coupled pseudospinor condensate with equal intra- and inter-species interactions against quantum and thermal fluctuations has been studied [40]. Berezinskii-Kosterlitz-Thouless (BKT) superfluid phase transition in an anisotropically SO-coupled two-dimensional pseudospinor BEC has been studied using a classical-field Monte Carlo calculations [41] and stochastic projected Gross-Pitaevskii equation [42]; the later study showed the emergence of a true long-range order in the relative phase sector and the quasi-long-range BKT order in the total phase sector [42].

In this work, we theoretically study the collective excitations of an SO-coupled spin-1 BEC, with antiferromagnetic spin-exchange interactions, in a quasi-one-dimensional harmonic trapping potential at zero and finite temperature using the Hartree-Fock-Bogoliubov (HFB) theory with Popov approximation. To the best of our knowledge, excitation spectra of SO-coupled spin-1 BECs in harmonic trapping potentials has neither been studied at zero nor at finite temperature. We calculate the collective excitation spectrum by numerically solving the generalized GP and Bogoliubov-de-Gennes (BdG) equations self consistently at zero and finite temperatures. In addition to this at  $T = 0$  K, we also calculate the collective oscillations by simulating the real-time propagation of the ground state using  $T = 0$  GP equations subjected to different kinds of spin and density perturbations. We also calculate the dispersion relation [43] to ascertain the nature of the excitations. To augment our numerical results, we use the variational method to calculate the frequencies of a few low-lying modes analytically.

The paper is organized as follows. In Sec. II, we describe the HFB theory with Popov approximation for an SO coupled spin-1 BEC in a quasi-one-dimensional trapping potential. In Sec. III A, we discuss the spectrum of the non-interacting SO-coupled spin-1 BEC. We calculate the collective excitations of SO-coupled spin-1 BEC of  $^{23}\text{Na}$  at zero temperature with and without SO coupling by solving the generalized GP and BdG equations in a self-consistent manner in Sec. III B and III C. In Sec. III D, we simulate the real-time dynamics of suitably perturbed ground state to monitor the dipole and breathing modes corresponding to density and spin channels, followed by a calculation of a few low-lying modes using variational method in Sec. III E. In Sec. IV, the excitation spectra at finite temperatures are discussed.

## II. MODEL

We consider a spin-1 SO-coupled spinor BEC in a highly anisotropic harmonic trapping potential  $V(x, y, z) = m(\omega_x^2 x^2 + \omega_y^2 y^2 + \omega_z^2 z^2)/2$ , where  $m$  is the atomic mass and  $\omega_y = \omega_z = \omega_\perp \gg \omega_x$ . The transverse degrees of free-

dom are then considered to be frozen, and the system is confined in the harmonic oscillator ground state along this direction with  $R_x \gg \xi \gg l_\perp$ , where  $R_x$  is the half-length of the condensate along  $x$  axis,  $\xi$  is the density-coherence length, and  $l_\perp = \sqrt{\hbar/m\omega_\perp}$ . In this case, we can integrate out the  $y$  and  $z$  coordinates from the condensate wave function and describe the system as a quasi-one-dimensional system along the  $x$  axis. This allows us to consider excitations only along the axial direction  $x$ . The grand-canonical Hamiltonian in the second-quantized form for a spin-1 BEC is  $\mathcal{H} = \mathcal{H}_0 + \mathcal{H}_{\text{int}}$ , where single-particle part of the Hamiltonian  $\mathcal{H}_0$  and interaction part of the Hamiltonian  $\mathcal{H}_{\text{int}}$  are [44, 45]

$$\mathcal{H}_0 = \int dx \hat{\psi}_i^\dagger [\mathcal{L}_{ij} - \iota \hbar \gamma f_x \partial_x] \hat{\psi}_j, \quad (1a)$$

$$\mathcal{H}_{\text{int}} = \int dx \left[ \frac{c_0}{2} \hat{\psi}_i^\dagger \hat{\psi}_j^\dagger \hat{\psi}_j \hat{\psi}_i + \frac{c_2}{2} \hat{\psi}_i^\dagger (f_\alpha)_{ij} \hat{\psi}_j \hat{\psi}_k^\dagger (f_\alpha)_{kl} \hat{\psi}_l \right], \quad (1b)$$

where  $\partial_x = \partial/\partial x$ ,  $\mathcal{L}_{ij} = [(-\hbar^2/2m)\partial_x^2 - \mu + V(x)] \delta_{ij}$ . In Eqs. (1a)-(1b),  $i, j, k, l$  which can have values  $+1, 0, -1$  are the hyperfine spin states of the  $F = 1$  manifold, repeated indices are summed over,  $f_\alpha$  with  $\alpha = x, y, z$  denote the spin-1 matrices in the irreducible representation,  $\hat{\psi}_i(x, t)$  ( $\hat{\psi}_i^\dagger(x, t)$ ) is the quantum field for annihilating (creating) an atom in state  $i$  at position  $x$ ,  $\mu$  is the chemical potential,  $\gamma$  is the strength of spin-orbit coupling, and  $c_0$  and  $c_2$  are spin-independent and spin-dependent interactions, respectively. The latter expressed in terms of the  $s$ -wave scattering lengths  $a_0$  and  $a_2$  of binary collisions with total spin  $F_{\text{total}} = 0$  and 2, respectively, are  $c_0 = 2\hbar^2(a_0 + 2a_2)/(3ml_\perp^2)$  and  $c_2 = 2\hbar^2(a_2 - a_0)/(3ml_\perp^2)$ . Depending on the values of  $c_2$ , a spin-1 BEC in the absence of SO coupling and Zeeman terms admits two phases, namely ferromagnetic for  $c_2 < 0$  and antiferromagnetic for  $c_2 > 0$ . In the rest of the manuscript, we will work with dimensionless variables (except when stated otherwise) defined as  $\tilde{x} = x/l_0$ ,  $\tilde{E} = E/\hbar\omega_x$ ,  $\tilde{t} = \omega_x t$ ,  $\tilde{\gamma} = \gamma/\sqrt{m\hbar\omega_x}$  and  $\tilde{c}_0 = 2(a_0 + 2a_2)l_0/(3l_\perp^2)$ ,  $\tilde{c}_2 = 2(a_2 - a_0)l_0/(3l_\perp^2)$ , where  $l_0 = \sqrt{\hbar/m\omega_x}$ ; we further denote the dimensionless variables without tilde in the rest of the manuscript.

## Fluctuations

To address the effects of quantum and thermal fluctuations in the BECs of dilute atomic gases, we generalize the HFB theory within the Popov approximation [46–48] and adapt it to an SO-coupled spin-1 Bose gas. We start with the second-quantized form of the Hamiltonian  $\mathcal{H}$  for a dilute, weakly-interacting Bose gas and derive the generalized GP and the BdG equations. We separate the Bose field operator  $\hat{\psi}_i(x, t)$  into a condensate wavefunction  $\phi_i(x)$  and a fluctuation operator  $\delta\hat{\psi}_i(x, t)$  as  $\hat{\psi}_i(x, t) = \phi_i(x) + \delta\hat{\psi}_i(x, t)$ . Employing the Bogoliubov transformation, fluctuation operators  $\delta\hat{\psi}_i$  can be expressed as a linear combination of quasi-particle creation

$(\hat{\alpha}_\lambda^\dagger)$  and annihilation operators  $(\hat{\alpha}_\lambda)$  given by

$$\delta\hat{\psi}_i(x, t) = \sum_\lambda \left[ u_i^\lambda(x) \hat{\alpha}_\lambda(x) e^{-i\omega_\lambda t} - v_i^{*\lambda}(x) \hat{\alpha}_\lambda^\dagger(x) e^{i\omega_\lambda t} \right], \quad (2)$$

where  $i \in (+1, 0, -1)$  represents the component index, and  $\lambda$  represents the eigenvalue index for the corresponding energy  $\omega_\lambda$  with  $u_i^\lambda$  and  $v_i^\lambda$  as the quasiparticle amplitudes of the  $i$ th component. The quasiparticle creation and annihilation operators satisfy the usual Bose commutation relations. We consider the Heisenberg equation for the Bose field operator  $\hat{\psi}_i(x, t)$ , i.e.,

$$i\hbar \frac{\partial}{\partial t} \hat{\psi}_i(x, t) = [\hat{\psi}_i(x, t), \mathcal{H}], \quad (3)$$

and then Wick decompose the cubic terms in fluctuation operators as  $\delta\hat{\psi}_i^\dagger \delta\hat{\psi}_j \delta\hat{\psi}_k \simeq \langle \delta\hat{\psi}_i^\dagger \delta\hat{\psi}_j \rangle \delta\hat{\psi}_k + \langle \delta\hat{\psi}_i^\dagger \delta\hat{\psi}_k \rangle \delta\hat{\psi}_j +$

$\langle \delta\hat{\psi}_j \delta\hat{\psi}_k \rangle \delta\hat{\psi}_i^\dagger$ . We consider the ensemble average of Eq. (3) and define  $n_i^c = |\phi_i|^2$ ,  $\tilde{n}_{i,j} \equiv \langle \delta\hat{\psi}_i^\dagger \delta\hat{\psi}_j \rangle$ ,  $\tilde{m}_{i,j} \equiv \langle \delta\hat{\psi}_i \delta\hat{\psi}_j \rangle$  and  $n_i = n_i^c + \tilde{n}_{i,i}$  as the local condensate, non-condensate, anomalous and total density, respectively, for the  $i$ th component and  $n_t = \sum_i (n_i^c + \tilde{n}_{i,i})$  as the total density of the system. To simplify the notation, we denote the thermal density of the  $i$ th component  $\tilde{n}_{i,i}$  as simply  $\tilde{n}_i$ . The anomalous average terms  $\tilde{m}_{i,j}$  are further neglected to satisfy the Hugenholtz-Pines theorem [49]. This forms the essence of Hartree-Fock-Bogoliubov-Popov approximation. Based on these considerations and definitions, we arrive at two coupled sets of equations, one for the condensate wavefunctions and second for quasiparticle amplitudes. One set of equations describing the dynamics of the condensate are the following coupled generalized GP equations

$$i \frac{\partial \phi_{\pm 1}}{\partial t} = [\mathcal{L}_{\pm 1, \pm 1} + c_0(n_t + \tilde{n}_{\pm 1, \pm 1}) + c_2(n_{\pm 1} + n_0 - n_{\mp 1} + \tilde{n}_{\pm 1, \pm 1})] \phi_{\pm 1} + c_2 \phi_0^2 \phi_{\mp 1}^* + [(c_0 + c_2) \tilde{n}_{0, \pm 1} + 2c_2 \tilde{n}_{\mp 1, 0}] \phi_0 + (c_0 - c_2) \tilde{n}_{\mp 1, \pm 1} \phi_{\mp 1} - i \frac{\gamma}{\sqrt{2}} \partial_x \phi_0, \quad (4a)$$

$$i \frac{\partial \phi_0}{\partial t} = [\mathcal{L}_{0,0} + c_0(n_t + \tilde{n}_{0,0}) + c_2(n_{+1} + n_{-1})] \phi_0 + 2c_2 \phi_{+1} \phi_0^* \phi_{-1} + [(c_0 + c_2) \tilde{n}_{+1,0} + 2c_2 \tilde{n}_{0,-1}] \phi_{+1} + [(c_0 + c_2) \tilde{n}_{-1,0} + 2c_2 \tilde{n}_{0,+1}] \phi_{-1} - i \frac{\gamma}{\sqrt{2}} (\partial_x \phi_{+1} + \partial_x \phi_{-1}). \quad (4b)$$

The BdG equations for quasiparticle amplitudes are given as

$$\begin{pmatrix} M_1 & -M_2 \\ M_2^* & -M_1^* \end{pmatrix} \begin{pmatrix} \mathbf{u}^\lambda \\ \mathbf{v}^\lambda \end{pmatrix} = \omega_\lambda \begin{pmatrix} \mathbf{u}^\lambda \\ \mathbf{v}^\lambda \end{pmatrix}, \quad (5)$$

where

$$M_1 = \begin{pmatrix} h_{+1,+1} + c_0 n_{+1} + c_2(2n_{+1} + n_0 - n_{-1}) & h_{+1,0} + h_{\text{soc}} & (c_0 - c_2)(\phi_{-1}^* \phi_{+1} + \tilde{n}_{-1,+1}) \\ h_{+1,0}^* + h_{\text{soc}} & h_{0,0} + c_0 n_0 + c_2(n_{+1} + n_{-1}) & h_{0,-1} + h_{\text{soc}} \\ (c_0 - c_2)(\phi_{+1}^* \phi_{-1} + \tilde{n}_{+1,-1}) & h_{0,-1}^* + h_{\text{soc}} & h_{-1,-1} + c_0 n_{-1} + c_2(n_0 - n_{+1} + 2n_{-1}) \end{pmatrix},$$

$$M_2 = \begin{pmatrix} (c_0 + c_2) \phi_{+1}^2 & (c_0 + c_2) \phi_0 \phi_{+1} & (c_0 - c_2) \phi_{-1} \phi_{+1} + c_2 \phi_0^2 \\ (c_0 + c_2) \phi_{+1} \phi_0 & c_0 \phi_0^2 + 2c_2 \phi_{+1} \phi_{-1} & (c_0 + c_2) \phi_{-1} \phi_0 \\ (c_0 - c_2) \phi_{+1} \phi_{-1} + c_2 \phi_0^2 & (c_0 + c_2) \phi_0 \phi_{-1} & (c_0 + c_2) \phi_{-1}^2 \end{pmatrix},$$

with

$$h_{i,j} = \left( -\frac{1}{2} \partial_x^2 - \mu + V(x) + c_0 n_t \right) \delta_{ij}, \quad h_{\text{soc}} = \frac{-i\gamma}{\sqrt{2}} \partial_x, \\ h_{+1,0} = (c_0 + c_2)(\phi_0^* \phi_{+1} + \tilde{n}_{0,+1}) + 2c_2(\phi_{-1}^* \phi_0 + \tilde{n}_{-1,0}), \\ h_{0,-1} = (c_0 + c_2)(\phi_0 \phi_{-1}^* + \tilde{n}_{-1,0}) + 2c_2(\phi_{+1} \phi_0^* + \tilde{n}_{0,+1}), \\ \mathbf{u}^\lambda = (u_{+1}^\lambda, u_0^\lambda, u_{-1}^\lambda)^\top, \quad \mathbf{v}^\lambda = (v_{+1}^\lambda, v_0^\lambda, v_{-1}^\lambda)^\top,$$

and  $\top$  denotes the transpose. The number density of the non-condensate atoms is related to the Bogoliubov quasiparticle

amplitudes through

$$\tilde{n}_{i,j} = \sum_{\lambda} \{ (u_i^{\lambda*} u_j^{\lambda} + v_i^{\lambda} v_j^{\lambda*}) f_{\omega_{\lambda}} + v_i^{\lambda} v_j^{\lambda*} \} \quad (6)$$

where  $f_{\omega_{\lambda}} = (e^{\omega_{\lambda}/k_B T} - 1)^{-1}$  is the Bose factor of the  $\lambda$ th quasiparticle state. Furthermore the quasiparticle amplitudes are normalized as  $\int \sum_i (|u_i^{\lambda}|^2 + |v_i^{\lambda}|^2) dx = 1$ , and total number of atoms is given by  $N = \int n_t dx$ . On diagonalizing Eq. (5), the energy of the collective excitations as well as the quasiparticle amplitudes are obtained. These can be used in Eq. (6) to obtain the non-condensate densities, which is eventually used in a self-consistent computation of Eqs. (4a)-(4b) and (5) to arrive at the condensate and the non-condensate densities. It is to be noted that when  $T \rightarrow 0$ , the Bose factor  $f_{\omega_{\lambda}} \rightarrow 0$ , and  $\tilde{n}_i$  reduces to  $\sum_{\lambda} |v_i^{\lambda}|^2$ , which accounts for the condensate depletion due to quantum fluctuations at  $T = 0$ . The stationary ground state solution at  $T = 0$  is numerically obtained following Refs. [50, 51] which serves as an initial input for computing the non-condensate densities. Using this solution and then discretizing Eq. (5) by finite difference methods [52], we cast Eq. (5) as a matrix eigenvalue equation and then solve using standard matrix diagonalization algorithms to obtain the eigen energies  $\omega_{\lambda}$  and quasiparticle amplitudes  $u_i^{\lambda}$  and  $v_i^{\lambda}$ . It is to be noted here that we have included the non-condensate density terms,  $\tilde{n}_{i,j}$  ( $i \neq j$ ), in the spin channel in the above equations. These coherence terms between the thermal atoms of different components have negligible contribution in scalar BECs but become important and comparable to the spin-dependent interaction terms in the case of spinor BECs. Furthermore, if one does not include these coherence terms, the excitation spectra for two SO coupling models, namely  $H_{\text{SOC}} = \gamma p_x f_x$  and  $H'_{\text{SOC}} = \gamma p_x f_z$ , which are related by a rotation about  $y$  axis by an angle  $\pi/2$  turn out to be different at finite as well as at zero temperature in the presence of quantum fluctuations. The inclusion of  $\tilde{n}_{ij}$  with  $i \neq j$  renders the excitation spectra for the two models equivalent which illustrates the important role of these terms in accounting for quantum and thermal fluctuations. In fact, even in the absence of SO coupling if these terms are not included, excitation spectrum of a polar spin-1 BEC is not equivalent to that of an antiferromagnetic BEC with same interaction

strengths in the presence of fluctuations. In this context, it is relevant to point out that these terms were not included in several studies on spin-1 BECs based on self-consistent solutions of Eqs. (4a)-(4b) and (5) [30, 53].

After calculating the collective excitations, one can also compute the associated wavenumbers, which essentially establishes the dispersion relation. We first compute  $\tilde{u}_i^{\lambda}(k)$  and  $\tilde{v}_i^{\lambda}(k)$ , the Fourier transforms of the Bogoliubov quasiparticle amplitudes  $u_i^{\lambda}(x)$  and  $v_i^{\lambda}(x)$ , respectively, and then calculate the root-mean-square wave number  $k_{\text{rms}}$  of the  $\lambda$ th quasiparticle mode as [43, 54, 55]

$$k_{\text{rms}}^{\lambda} = \sqrt{\frac{\sum_i \int dk k^2 [|\tilde{u}_i^{\lambda}(k)|^2 + |\tilde{v}_i^{\lambda}(k)|^2]}{\sum_i \int dk [|\tilde{u}_i^{\lambda}(k)|^2 + |\tilde{v}_i^{\lambda}(k)|^2]}}. \quad (7)$$

In Sec. III, we shall demonstrate that density and spin modes have distinct dispersion curves.

### III. COLLECTIVE EXCITATIONS AT ZERO TEMPERATURE

#### A. Non-interacting spin-1 BEC

We first analyze the spectrum of the single particle SO-coupled Hamiltonian

$$H_0 = \mathbb{1} \times \left[ -\frac{1}{2} \partial_x^2 + \frac{x^2}{2} - \mu \right] - \iota \gamma f_x \partial_x, \quad (8)$$

where  $\mathbb{1}$  is a  $3 \times 3$  identity matrix. As  $H_0$  and  $U^{\dagger} H_0 U$ , where  $U$  is a unitary operator, have identical spectra, we consider the  $U^{\dagger} H_0 U$  with  $U$  defined as a rotation operator which rotates the spin state of a spin-1 particle about  $y$  by an angle  $\pi/2$  in an anticlockwise direction. The unitary operator  $U$  is defined as

$$U = \begin{pmatrix} 1/2 & -1/\sqrt{2} & 1/2 \\ 1/\sqrt{2} & 0 & -1/\sqrt{2} \\ 1/2 & 1/\sqrt{2} & 1/2 \end{pmatrix}. \quad (9)$$

The  $U^{\dagger} H_0 U$  thus obtained in momentum space is

$$\begin{pmatrix} -\frac{1}{2} \frac{\partial^2}{\partial k^2} + \frac{(k+\gamma)^2}{2} - \frac{\gamma^2}{2} - \mu & 0 & 0 \\ 0 & -\frac{1}{2} \frac{\partial^2}{\partial k^2} + \frac{k^2}{2} - \mu & 0 \\ 0 & 0 & -\frac{1}{2} \frac{\partial^2}{\partial k^2} + \frac{(k-\gamma)^2}{2} - \frac{\gamma^2}{2} - \mu \end{pmatrix},$$

with eigen functions

$$\begin{pmatrix} \frac{1}{\sqrt{2^n \sqrt{\pi n!}}} \exp\left(\frac{-(k+\gamma)^2}{2}\right) H_n(k) \\ 0 \\ 0 \end{pmatrix}, \begin{pmatrix} \frac{1}{\sqrt{2^n \sqrt{\pi n!}}} \exp\left(\frac{-k^2}{2}\right) H_n(k) \\ 0 \\ 0 \end{pmatrix}, \begin{pmatrix} 0 \\ 0 \\ \frac{1}{\sqrt{2^n \sqrt{\pi n!}}} \exp\left(\frac{-(k-\gamma)^2}{2}\right) H_n(k) \end{pmatrix} \quad (10)$$

and eigen spectrum

$$\epsilon_{\pm 1}(n) = \left(n + \frac{1}{2}\right) - \frac{\gamma^2}{2} - \mu, \quad \epsilon_0(n) = \left(n + \frac{1}{2}\right) - \mu, \quad (11)$$

where  $n = 0, 1, 2, \dots$ ,  $\mu = (1 - \gamma^2)/2$ , and  $H_n(k)$  is the Fourier transform of  $n$ th order Hermite polynomial. So we

get two degenerate eigen functions and the third is shifted up by  $\gamma^2/2$  for each value  $n$ . In the absence of a trap, the energy dispersion is

$$\epsilon_{\pm 1}(k) = \frac{(k \pm \gamma)^2}{2} - \frac{\gamma^2}{2} - \mu, \quad \epsilon_0(k) = \frac{k^2}{2} - \mu, \quad (12)$$

where  $\mu$  would be fixed by the number density. The effect of SO coupling is, therefore, to open a gap and also shift the minima of  $\epsilon_{\pm 1}$  with respect to  $\epsilon_0$ . The eigen functions of  $H_0$  corresponding to eigen energies  $\epsilon_{\pm 1}(n)$  and  $\epsilon_0(n)$  are, respectively,

$$\frac{1}{\sqrt{2^n \sqrt{\pi} n!}} \exp(-\{x/2 \pm i\gamma\}x) H_n(x) \begin{pmatrix} 1/2 \\ \pm 1/\sqrt{2} \\ 1/2 \end{pmatrix}, \quad (13)$$

$$\frac{1}{\sqrt{2^n \sqrt{\pi} n!}} \exp(-x^2/2) H_n(x) \begin{pmatrix} -1/\sqrt{2} \\ 0 \\ 1/\sqrt{2} \end{pmatrix}. \quad (14)$$

### B. Interacting spin-1 BEC without SO coupling

We now discuss the role of contact interactions on the ground state of spin-1 spinor condensates at  $T = 0$  K and associated excitation spectra in the absence of spin-orbit coupling and quantum fluctuations. In particular, as a representative example, we consider the antiferromagnetic phase of  $^{23}\text{Na}$  [1] atoms in the  $F = 1$  manifold confined in a cigar-shaped trapping potential with the trapping parameters  $\omega_x = 2\pi \times 5$  Hz,  $\omega_y = \omega_z = 20\omega_x$ , and having scattering lengths  $a_0 = 48.91a_B$  and  $a_2 = 54.54a_B$  [56], where  $a_B$  is the Bohr radius. The interaction strengths, in dimensionless units, translate to  $c_0 = 0.0119N$  and  $c_2 = 0.000424N$ . With an increase in the number of atoms, the spatial extent of the ground-state density profiles increases. The antiferromagnetic order constrains zero population in  $m_f = 0$  hyperfine state but with an equal population in the  $m_f = 1$  and  $m_f = -1$  states or all the atoms in  $m_f = 0$  state. The longitudinal magnetization  $M_z = \int dx (|\phi_{+1}|^2 - |\phi_{-1}|^2)$  is hence equal to zero. We further investigate the excitation spectrum of the antiferromagnetic phase which is accomplished by diagonalizing the BdG matrix in (5). In Fig. 1, we show the variation in the excitation frequencies with total number of atoms  $N$ . For a single particle, i.e., when the interactions are absent, the excitation spectrum is exactly equivalent to the spectra of three independent harmonic oscillators. However, in the presence of interactions the equations get coupled. Here the spectrum is characterized by the three Goldstone modes with zero excitation frequency. These modes also serve as a self-consistency check for the accuracy of our numerical calculations. The presence of three Goldstone modes is attributed to the fact that for the antiferromagnetic phase, the symmetry group is  $U(1) \times S^2$  [44] such that we can have three broken symmetries. Apart from the one *density* Goldstone mode arising out of the breaking of  $U(1)$  gauge symmetry, the other two *spin* Goldstone modes emanate from the breaking of two symmetry generators of the spin rotation [57]. Among the non-zero low-lying

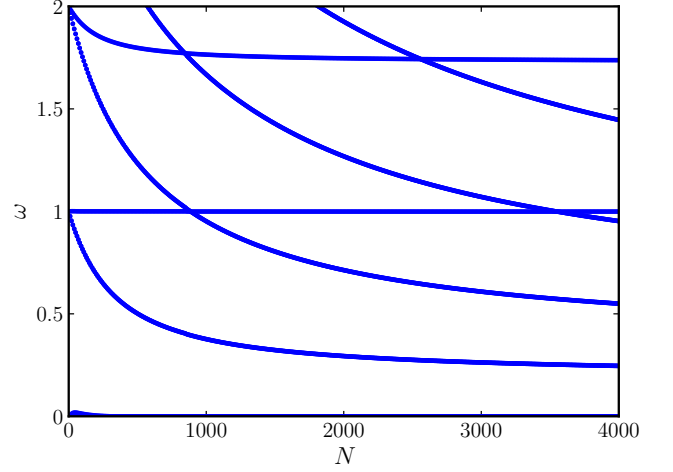


FIG. 1. Low-lying excitation spectrum for  $^{23}\text{Na}$  spin-1 BEC with  $c_0 = 0.0119N$ ,  $c_2 = 0.000424N$ , and  $\gamma = 0$  as a function of number of atoms  $N$  at zero temperature. Each set of three degenerate modes in the non-interacting limit splits into two branches in the presence of interactions: the low lying branch consists of two degenerate spin modes and the other corresponds to a single density mode.

modes, with introduction of the interactions, the degeneracy between the modes with  $\omega = 1$  is lifted with a bifurcation into two branches. One branch corresponds to the density-dipole mode whose energy remains constant with increasing  $N$  satisfying the Kohn's theorem [58]. The other branch consists of two degenerate spin dipole modes. At the outset with an increase in  $N$ , the energy of these spin modes decreases sharply, and then gets saturated for higher values of  $N$ . Similarly, three degenerate modes with  $\omega = n$  for a non-interacting system where  $n = 2, 3, \dots$  lead to two degenerate spin modes and a density mode having energy higher than corresponding spin modes with the introduction of interactions as shown in Fig. 1.

### C. Interacting spin-1 BEC with SO coupling

In Fig. 2, we show the variation in the excitation frequencies as a function of total number of atoms  $N$  with fixed SO coupling strength ( $\gamma = 0.5$ ). The excitation spectrum is characterized by two zero-energy modes which are identified as two Goldstone modes. One of these is a density Goldstone mode arising out of the breaking of  $U(1)$  gauge symmetry and the other is a spin Goldstone mode originating from the breaking of global  $SO(2)$  spin-space rotation symmetry [14]. For a small number of atoms, the first non-zero mode is shifted approximately by  $\gamma^2/2$  as shown in Fig. 2. Among the non-zero low lying modes, in the presence of SO coupling, is the density-dipole mode, with frequency  $\omega = 1$ , which remains constant with increasing  $N$  satisfying Kohn's theorem. Another consequence of SO coupling is the lifting of the degeneracy between two spin modes as can be seen by comparing Figs. 1 and 2. On increasing the interaction strengths, the en-

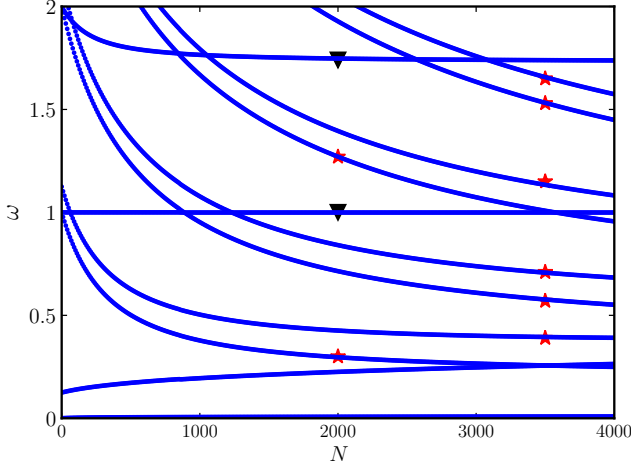


FIG. 2. Excitation spectrum for  $^{23}\text{Na}$  spin-1 BEC with  $c_0 = 0.0119N$ ,  $c_2 = 0.000424N$  and  $\gamma = 0.5$  as a function of number of atoms  $N$  at zero temperature. The two degenerate modes in the non-interacting limit, bifurcate with the energy of the spin mode (marked with red stars) becoming lower than the corresponding density mode (marked with black triangles).

$$\begin{pmatrix} A + \iota\gamma\partial_x & -B & C & -D \\ B^* & -A + \iota\gamma\partial_x & D^* & C^* \\ C^* & -D & E - \iota\gamma\partial_x & -F \\ D^* & -C & F^* & -E - \iota\gamma\partial_x \end{pmatrix} \begin{pmatrix} u_{\pm 1}^\lambda \\ v_{\pm 1}^\lambda \\ u_{\mp 1}^\lambda \\ v_{\mp 1}^\lambda \end{pmatrix} = \omega_{\pm\lambda} \begin{pmatrix} u_{\pm 1}^\lambda \\ v_{\pm 1}^\lambda \\ u_{\mp 1}^\lambda \\ v_{\mp 1}^\lambda \end{pmatrix}, \quad (15)$$

where

$$\begin{aligned} A &= \left(-\frac{1}{2}\partial_x^2 - \mu + V(x)\right) + 2(c_0 + c_2)n_{+1}^c \\ &\quad + (c_0 - c_2)n_{-1}^c, \quad B = (c_0 + c_2)\phi_{+1}^2, \\ C &= (c_0 - c_2)\phi_{+1}\phi_{-1}^*, \quad D = (c_0 - c_2)\phi_{+1}\phi_{-1}, \\ E &= \left(-\frac{1}{2}\partial_x^2 - \mu + V(x)\right) + 2(c_0 + c_2)n_{-1}^c \\ &\quad + (c_0 - c_2)n_{+1}^c, \quad F = (c_0 + c_2)\phi_{-1}^2. \end{aligned}$$

and that for  $(u_0^\lambda, v_0^\lambda)$  is

$$\begin{pmatrix} R & -S \\ S^* & -R \end{pmatrix} \begin{pmatrix} u_0^\lambda \\ v_0^\lambda \end{pmatrix} = \omega_{0\lambda} \begin{pmatrix} u_0^\lambda \\ v_0^\lambda \end{pmatrix}, \quad (16)$$

where  $R = [-\partial_x^2/2 - \mu + V(x)] + (c_0 + c_2)(n_{+1}^c + n_{-1}^c)$  and  $S = 2c_2\phi_{+1}\phi_{-1}$ . Eq. (15) is same as the BdG equations of a pseudospinor-1/2 BEC consisting of  $m_f = \pm 1$  components with an SO coupling of  $\gamma p_x \sigma_z$ , where  $\sigma_z$  is a Pauli spin matrix for spin-1/2 system. Moreover, the eigen modes in (16) are shifted upwards by  $\gamma^2/2$  compared to the spin mode in (15). As mentioned earlier, spin-1 BEC with  $H_{\text{SOC}}$  and  $H'_{\text{SOC}}$  have identical spectra; the quasiparticle amplitudes with the former can be obtained from a unitary transformation, defined by  $U$

ergy of these non-degenerate spin modes decreases, and then gets saturated for higher values of  $N$ . The energy separation between these two spin modes remains approximately equal to  $\gamma^2/2$  with a variation in the number of atoms. As expected, for a fixed value of  $N$ , increasing  $\gamma$  increases the energy of one of the spin modes in the pair, whereas the energy of the other spin and density modes remain unchanged. This is demonstrated in Fig. 3 where excitation spectrum as a function of SO-coupling strength is plotted. The modes which are bifurcating from  $\gamma = 0$  in Fig. 3 are the spin modes, while the remaining modes are the density modes.

To further understand the role of SO coupling on the excitation spectrum, we consider  $H'_{\text{SOC}} = \gamma p_x f_z$ , where the absence of  $m_f = 0$  component as shown in Fig. 4(a) at  $T = 0$  K results in the decoupling of the BdG Eqs. (5) corresponding to quasiparticle amplitudes  $(u_{\pm 1}^\lambda, v_{\pm 1}^\lambda)$  from those for  $(u_0^\lambda, v_0^\lambda)$ . On the other hand, for  $H_{\text{SOC}} = \gamma p_x f_x$  all  $m_f = 0, \pm 1$  components are non-zero as shown in Fig. 4(b) [14]. The solution shown in Fig. 4(b) can be obtained by operating  $U$  in Eq. (9) on the solution shown in Fig. 4(a). The resultant eigen value equation for  $(u_{\pm 1}^\lambda, v_{\pm 1}^\lambda)$  with  $H'_{\text{SOC}} = \gamma p_x f_z$  is

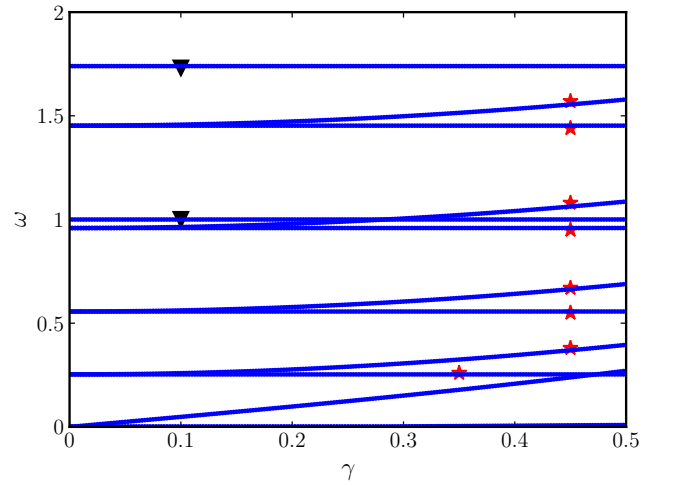


FIG. 3. Excitation spectrum for  $^{23}\text{Na}$  spin-1 BEC with  $c_0 = 0.0119N$ ,  $c_2 = 0.000424N$  and  $N = 4000$  as a function of SO coupling strength  $\gamma$  at zero temperature. The modes bifurcating from  $\gamma = 0$  are the spin modes (marked with red stars), whereas the remaining modes not changing with a variation in  $\gamma$  are density modes (marked with black triangles).

in (9), of the quasiparticle amplitudes for the latter. In Sec.

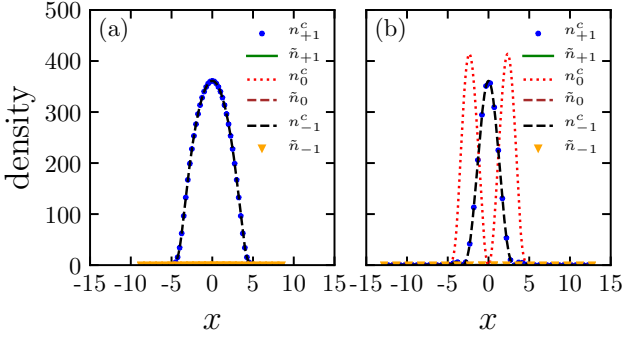


FIG. 4. (a) Condensate densities,  $n_i^c(x)$ , and thermal densities,  $\tilde{n}_i(x)$ , for a  $^{23}\text{Na}$  spin-1 BEC with  $c_0 = 0.0119N$ ,  $c_2 = 0.000424N$ ,  $N = 4000$ ,  $\gamma = 0.5$  and SO coupling  $H'_{\text{soc}} = \gamma f_z p_x$ . The same for  $H_{\text{soc}} = \gamma f_x p_x$  are shown in (b).

III E, we use the variational method to calculate a few low-lying modes corresponding to Eq. (15).

To understand the breakdown in the degeneracy between the pairs of spin modes in the presence of SO coupling, we analyse their Bogoliubov amplitudes and phases. As an example in Figs. 5(a) and (b), the Bogoliubov amplitudes of the two

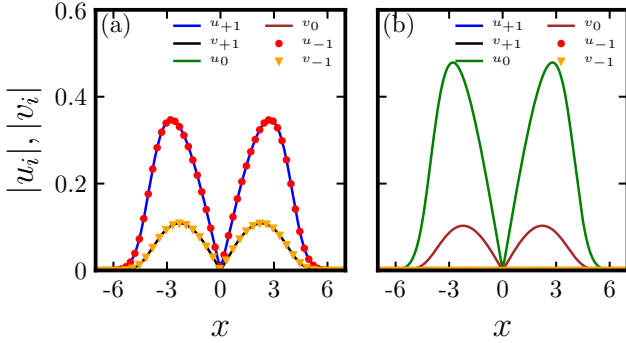


FIG. 5. (a) and (b) The Bogoliubov amplitudes for the spin-dipole modes with  $c_0 = 0.0119N$ ,  $c_2 = 0.000424N$ ,  $N = 4000$  without and with  $H'_{\text{soc}} = \gamma f_z p_x$ . Without SO coupling, (a) and (b) show  $|u_i|$  and  $|v_i|$ s for two degenerate spin-dipole modes. These are also identical to the spin-dipole modes in the presence of  $H'_{\text{soc}} = 0.5 f_z p_x$ , where (a) and (b) are equivalent to the amplitudes for the spin-dipole modes with lower and higher frequency, respectively.

spin-dipole modes for  $c_0 = 0.0119N$ ,  $c_2 = 0.000424N$  with  $N = 4000$  are plotted. The  $|u_i|$  and  $|v_i|$ s for the two modes are identical without and with  $\gamma f_z p_x$  SO coupling. The excitation frequencies of the modes with  $\gamma = 0$  and  $\gamma = 0.5$  are already shown in Fig. 1 and Fig. 2, respectively. The phase profiles corresponding to the Bogoliubov amplitudes in Figs. 5(a) and (b) with  $\gamma = 0$  are shown in Figs. 6(a) and (b), respectively, whereas the same with  $H'_{\text{soc}} = 0.5 f_z p_x$  are shown in Figs. 6(c) and (d), respectively. With SO coupling the mode with lower excitation frequency acquires SO-coupling strength-dependent phase gradient, whereas the phase-profile of the mode with higher excitation frequency remains un-

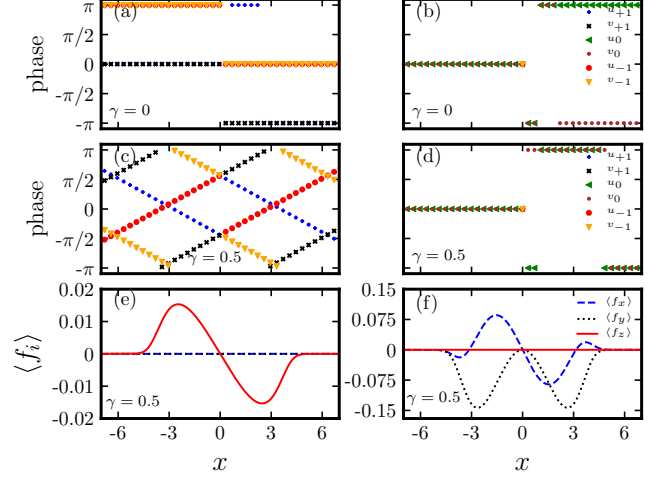


FIG. 6. (a), (b) The phase profiles of the spin-dipole modes in the absence of SO coupling corresponding to the Bogoliubov amplitudes shown in Figs. 5(a), (b). (c) and (d) show the corresponding phase profiles with  $H'_{\text{soc}} = 0.5 f_z p_x$  of the lower and higher frequency spin-dipole modes. (e) and (f) are the spin textures corresponding to the lower and higher frequency spin-dipole modes in the presence of  $H'_{\text{soc}} = 0.5 f_z p_x$ . Here  $\langle \dots \rangle$  represents the expectation with respect to the perturbed order parameter.

changed. Without SO coupling these Bogoliubov modes can be transformed from one to another by a rotation in spin space about  $y$  axis by an angle  $\pi/2$ , whereas in the presence of SO coupling the modes are not connected by such a unitary transformation. The breakdown in degeneracy of the spin-dipole modes is also accompanied by distinct spin-density vectors ( $\mathbf{f} = (\langle f_x \rangle, \langle f_y \rangle, \langle f_z \rangle)$ ) as shown in Figs. 6(e) and (f) for lower and higher frequency spin modes, respectively.

We have also numerically computed the dispersion curves for the system as shown in Fig. 7. For the spin-1 BEC, the spin-independent interaction strength is higher than the spin-dependent interaction strength making the energy of density excitations greater than the spin excitations for any given  $k_{\text{rms}}$  as shown in Fig. 7(a) in the absence of SO coupling. In Fig. 7(a), the dispersion for the two spin modes overlap indicating the degeneracy between the modes. Furthermore, the presence of SO coupling lifts the degeneracy between these modes as is shown in Fig. 7(b). The dispersion in the presence and absence of SO coupling are consistent with the excitation spectra in Figs. (1) and (2), respectively.

#### D. Dynamics

In order to examine the nature of the low-lying collective excitations through physical observables and validate our theoretical predictions of mode frequencies obtained from the BdG equations, we perform direct numerical dynamical real-time simulations of the system by evolving the ground state with appropriate perturbations. The time evolution is done using  $T = 0$  K coupled GP equations. This type of proce-

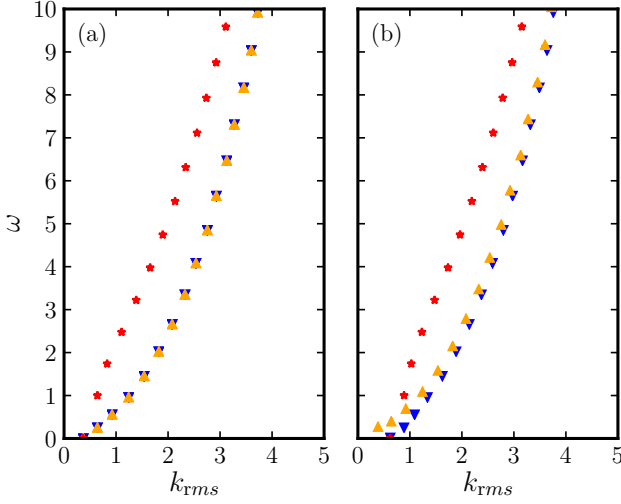


FIG. 7. (a) Dispersion curves of the  $^{23}\text{Na}$  spin-1 BEC with  $c_0 = 0.0119N$ ,  $c_2 = 0.000424N$ ,  $N = 4000$ , and  $\gamma = 0$ . The same for  $\gamma = 0.5$  are shown in (b). Red stars represent the dispersion for the density modes, whereas upper and lower triangles correspond to dispersion for spin modes. The lifting of degeneracy between the spin modes in the presence of SO coupling results in three distinct dispersion branches in (b).

ture has already been used experimentally to study low-lying collective excitations by modulating the trapping potential for density [21] and spin-dipole modes [59]. We, however, use perturbation by constructing the fluctuation operator corresponding to the dipole and breathing modes in the density and spin channels. The fluctuation is constructed with the Bogoliubov quasiparticle amplitudes  $u$ s and  $v$ s corresponding to the frequency  $\omega$  of the relevant mode. To execute, we add the fluctuation  $\delta\psi_i \propto (u_i^\lambda - v_i^{*\lambda})$  to the ground state wave function at time  $t = 0$  to excite a mode with frequency  $\omega_\lambda$ . The system is then evolved and a relevant physical observable is monitored over time. We consider  $^{23}\text{Na}$  spin-1 BEC consisting of 4000 atoms with  $c_0 = 0.0119N$ ,  $c_2 = 0.000434N$  and with a SO coupling  $H'_{\text{SOC}} = \gamma p_x f_z$ , where  $\gamma = 0.5$  in the remainder of this subsection.

**Density-dipole and breathing modes:** To excite the density-dipole mode, we study the center of mass motion via  $x_{\text{CM}}(t) = \langle x \rangle = \sum_{i=-1,0,+1} \int x |\phi_i(x,t)|^2 dx$ , where  $\langle \dots \rangle$  corresponds to an expectation with respect to the time-evolved ground-state. In Fig. 8 (a), we plot the time dependence of  $x_{\text{CM}}(t)$ . We compute the Fourier transform (FT) of  $x_{\text{CM}}(t)$  to demonstrate that the dominant frequency resonates at  $\omega = 1$ ; the FT is shown in Fig. 8 (b). Experimentally, the density-dipole mode is excited by a translational shift in the external trapping potential [21]. Furthermore, to examine the excitation of the breathing mode, we consider the corresponding observable  $x^2$  and calculate mean square radius  $x_{\text{ms}}^2(t) = \langle x^2 \rangle = \sum_{i=-1,0,+1} \int x^2 |\phi_i(x,t)|^2 dx$  as a function of time. In Fig. 8 (c) and (d), we show the variation in  $x_{\text{ms}}^2(t)$  and the most dominant peak at  $\omega = 1.73$  in the FT of  $x_{\text{ms}}^2(t)$ . The density-breathing mode can also be excited by perturbing

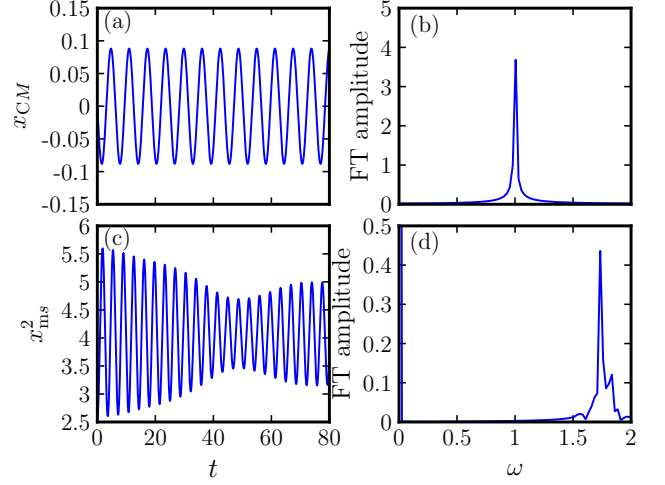


FIG. 8. (a) shows the center of mass oscillations, i.e.,  $x_{\text{CM}}(t)$  as a function of time and (b) the Fourier transform of  $x_{\text{CM}}(t)$  with a dominant peak at  $\omega = 1$ . Similarly, (c) shows the oscillations in the mean square size of the system,  $x_{\text{ms}}^2(t)$ , and (d) the Fourier transform of  $x_{\text{ms}}^2(t)$  with a dominant peak at  $\omega = 1.73$ . The dynamics corresponds  $^{23}\text{Na}$  spin-1 BEC consisting of 4000 atoms with  $c_0 = 0.0119N$ ,  $c_2 = 0.000424N$  and  $\gamma = 0.5$ . Both (a) and (c) represent the density excitations.

the trap strength [21]. It is worth mentioning here that the frequency of oscillations obtained from the real-time dynamics indeed agrees quite well with the corresponding collective excitations obtained from the equilibrium BdG analysis as shown in Fig. 2 for  $N = 4000$  and  $\gamma = 0.5$ .

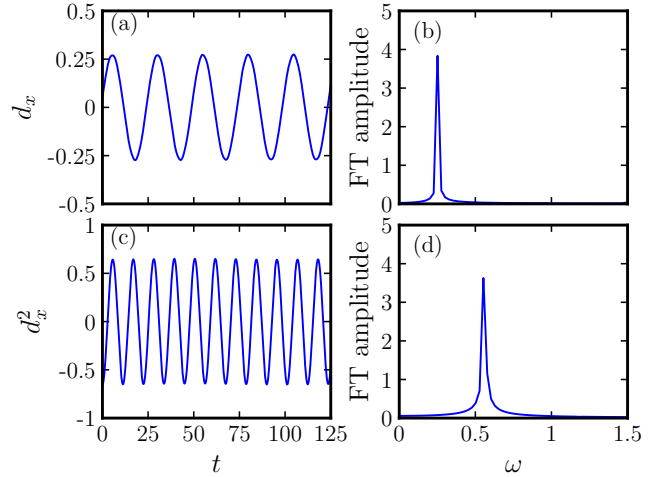


FIG. 9. Plots showing (a)  $d_x(t) = \langle x f_z \rangle$  as a function of time and (b) the Fourier transform of  $d_x(t)$  with a dominant peak at  $\omega = 0.25$ . (c) and (d) are the same for  $d_x^2(t) = \langle x^2 f_z \rangle$  and its Fourier transform with a dominant peak at  $\omega = 0.55$ , respectively. The peaks in (b) and (d) are the frequencies of spin-dipole and spin-breathing modes, respectively. The dynamics corresponds  $^{23}\text{Na}$  spin-1 BEC consisting of 4000 atoms with  $c_0 = 0.0119N$ ,  $c_2 = 0.000424N$  and  $\gamma = 0.5$ . Both (a) and (c) represent the spin excitations.

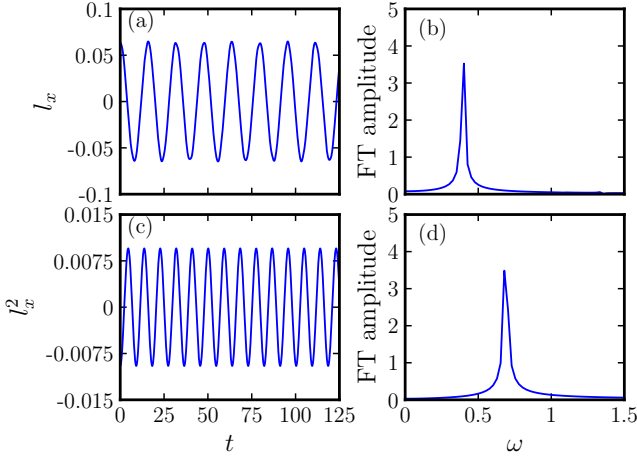


FIG. 10. Plots showing (a)  $l_x(t) = \langle x f_x \rangle$  as a function of time and (b) the Fourier transform of  $l_x(t)$  with a dominant peak at  $\omega = 0.395$ . (c) and (d) are the same for  $l_x^2(t) = \langle x^2 f_x \rangle$  and its Fourier transform with a dominant peak at  $\omega = 0.685$ , respectively. The peaks in (b) and (d) are the frequencies of SSD and SSB modes, respectively. The dynamics corresponds  $^{23}\text{Na}$  spin-1 BEC consisting of 4000 atoms with  $c_0 = 0.0119N$ ,  $c_2 = 0.000424N$  and  $\gamma = 0.5$ . Both (a) and (c) represent the spin excitations.

*Spin-dipole and spin-breathing modes:* We now turn our attention to excite the spin channel where we first choose the observable  $x f_z$  which corresponds to the spin-dipole mode. We study the dynamics of  $d_x(t) = \langle x f_z \rangle = \int \phi_i^*(x, t) (x f_z)_{ij} \phi_j(x, t) dx = \sum_{i=-1,1} \int x |\phi_i(x, t)|^2 dx$ . In Fig. 9 (a), we plot time dependence of  $d_x$  and in Fig. 9 (b) the frequency dependence of the FT of  $d_x$  with a primary peak at  $\omega = 0.25$ . Similarly, the spin-breathing mode corresponds to observable  $x^2 f_z$ . In Fig. 9 (c) and (d), we show the dynamics of  $d_x^2 = \langle x^2 f_z \rangle = \sum_{i=-1,1} \int x^2 |\phi_i(x, t)|^2 dx$ , i.e., the relative difference in the mean-square radii of the  $m_f = \pm 1$  components and the associated FT with a dominant peak at  $\omega = 0.55$ , respectively. The frequencies of oscillations thus obtained from the dynamics conform to the BdG analysis of the antiferromagnetic spinor condensates at equilibrium as illustrated in Fig. 2 for  $N = 4000$  and  $\gamma = 0.5$ .

*Shifted spin-dipole and spin-breathing modes:* We now discuss the excitation of the spin modes whose energies increase with an increase in SO coupling strength as discussed in Sec. III C. As mentioned earlier, these are precisely the modes appearing in Eq. (16). Here we first consider the observable  $x f_x$  corresponding to the shifted spin-dipole mode (SSD) and study the time-dependence of its expectation, i.e.,  $l_x(t) = \int \phi_i^*(x, t) (x f_x)_{ij} \phi_j(x, t) dx$ . We show  $l_x(t)$  as a function of  $t$  and the frequency dependence of its FT with a primary peak at  $\omega = 0.395$  in Figs. 10(a) and (b), respectively. Similarly, the shifted spin-breathing mode (SSB) corresponds to the observable  $x^2 f_x$ . In Fig. 10 (c) and (d), we illustrate the dynamics of  $l_x^2(t) = \langle x^2 f_x \rangle = \int \phi_i^*(x, t) (x^2 f_x)_{ij} \phi_j(x, t) dx$  and the corresponding FT with a dominant peak at  $\omega = 0.685$ , respectively. The frequencies of oscillations thus obtained from the dynamics, i.e., 0.395 and 0.685 for SSD and SSB, respectively, agree very well with the BdG analysis of the anti-

ferromagnetic spinor condensates at equilibrium as illustrated in Fig. 2 for  $N = 4000$  and  $\gamma = 0.5$ .

All of these modes can also be excited for  $H_{\text{SOC}} = \gamma p_x f_x$  with exactly the same excitation frequencies. The relevant observable in this case can be obtained by a transformation  $U \hat{O} U^\dagger$ , where  $\hat{O}$  is the observable for  $H'_{\text{SOC}} = \gamma p_x f_z$ . It implies that with  $H_{\text{SOC}}$ , the observable for the density modes will remain the same, i.e.,  $x$  and  $x^2$  for density-dipole and density-breathing modes, respectively. On the other hand, the observables for spin-dipole and spin-breathing modes are  $x f_x$  and  $x^2 f_x$ , respectively, while for the shifted spin-dipole and spin-breathing modes, operators are  $x f_z$  and  $x^2 f_z$ , respectively.

### E. Variational analysis

For a quasi-one-dimensional spin-1 BEC the spectrum of the low-energy excitations can be studied by using a time-dependent variational method introduced in Ref. [60, 61]. For simplicity, we have considered  $H'_{\text{SOC}} = \gamma p_x f_z$  which as discussed earlier allows the spectrum analysis as a composition of the spectra of two subsystems: one of which corresponds to a pseudospin-1/2 BEC of  $m_f = \pm 1$  components with  $\gamma p_x \sigma_z$  SO coupling and the second corresponding to the excitation in  $m_f = 0$  component of SO-coupled spin-1 BEC. We calculate a few low lying modes of the pseudospinor sub-system using the variational method. We consider the Gaussian variational ansatz

$$\phi_{\pm 1}(x, t) = A(t) \exp \left[ -\frac{\{x - x_{\pm 1}(t)\}^2}{2\sigma(t)^2} + i\alpha_{\pm 1}(t) \{x - x_{\pm 1}(t)\} + i\beta(t) \{x - x_{\pm 1}(t)\}^2 \right], \quad (17)$$

where  $\sigma$ ,  $x_{\pm 1}$ ,  $\alpha_{\pm 1}$  and  $\beta$  denoting the condensate width, displacement of the  $m_f = \pm 1$  components from the center of a harmonic trap, phase-gradient and chirp, respectively, are the time-dependent variational parameters. The Lagrangian of the subsystem is

$$L = \int \sum_{j=-1,+1} dx \frac{t}{2} \left( \phi_j^* \frac{\partial \phi_j}{\partial t} - \phi_j \frac{\partial \phi_j^*}{\partial t} \right) - E \quad (18)$$

where energy  $E$  is defined as

$$E = N \int_{-\infty}^{\infty} \left\{ \sum_{j=-1,+1} \left( \frac{1}{2} \left| \frac{d\phi_j}{dx} \right|^2 + V n_j^c \right) + \frac{c_0}{2} (n_{+1}^c + n_{-1}^c)^2 + \frac{c_2}{2} (n_{+1}^c - n_{-1}^c) n_{+1}^c + \frac{c_2}{2} (n_{-1}^c - n_{+1}^c) n_{-1}^c + \gamma \left( -i\phi_{+1}^* \frac{d\phi_{+1}}{dx} + i\phi_{-1}^* \frac{d\phi_{-1}}{dx} \right) \right\} dx. \quad (19)$$

We insert Eq. (17) in Eq. (18) and then compute the Euler-Lagrange equations. The Euler-Lagrange equations for the phase-gradients are  $\alpha_{\pm 1} = m\dot{x}_{\pm 1}/\hbar$  and for the chirp is  $\beta = \dot{\sigma}/2\sigma$ , which are then used in the equation of motion for  $x_{\pm 1}$  and condensate width  $\sigma$  respectively. After linearizing the resultant Euler's equations, we get the following equations of motion

$$\delta\ddot{\sigma}(t) + \delta\sigma(t) = -\sqrt{\frac{2}{\pi}} \frac{c_0}{\sigma^3} \delta\sigma(t) - \frac{3}{\sigma^4} \delta\sigma(t) + \frac{\sqrt{2}}{\pi} \frac{(c_0 - c_2)}{\sigma^5} (x_{+1} - x_{-1})^2 \delta\sigma(t) - \frac{1}{\sqrt{2\pi}} \frac{(c_0 - c_2)}{\sigma^4} (x_{+1} - x_{-1}) (\delta x_{+1}(t) - \delta x_{-1}(t)), \quad (20a)$$

$$\delta\ddot{x}_{+1}(t) + \delta x_{+1}(t) = \frac{1}{2\sqrt{2\pi}} \frac{(c_0 - c_2)}{\sigma^3} (\delta x_{+1}(t) - \delta x_{-1}(t)) - \frac{3}{2\sqrt{2\pi}} \frac{(c_0 - c_2)}{\sigma^4} \delta\sigma(t) (x_{+1} - x_{-1}), \quad (20b)$$

$$\delta\ddot{x}_{-1}(t) + \delta x_{-1}(t) = -\frac{1}{2\sqrt{2\pi}} \frac{(c_0 - c_2)}{\sigma^3} (\delta x_{+1}(t) - \delta x_{-1}(t)) + \frac{3}{2\sqrt{2\pi}} \frac{(c_0 - c_2)}{\sigma^4} \delta\sigma(t) (x_{+1} - x_{-1}). \quad (20c)$$

where  $\sigma$  and  $x_{\pm 1}$  are to be understood as the equilibrium values. For breathing oscillation, we consider  $\delta x_{\pm 1}(t) = 0$ . The equation of motion from (20a) for the condensate width  $\sigma$  results in

$$\ddot{\delta\sigma}(t) + \left(1 + \frac{3}{\sigma^4} + \sqrt{\frac{2}{\pi}} \frac{c_0}{\sigma^3}\right) \delta\sigma(t) = 0. \quad (21)$$

The equilibrium width ( $\sigma$ ) of the condensate satisfies

$$\sigma^4 - \frac{c_0\sigma}{\sqrt{2\pi}} = 1, \quad (22)$$

and eigen frequency of the oscillations in the width about its equilibrium value is

$$\omega_b = \left[1 + \frac{3}{\sigma^4} + \sqrt{\frac{2}{\pi}} \frac{c_0}{\sigma^3}\right]^{1/2} \quad (23)$$

which is equal to 1.737 for  $c_0 = 0.0119N$  with  $N = 4000$ . The variational result matches with density-breathing mode of the BdG spectrum shown in Fig. 2. For dipole and spin dipole oscillation, we consider  $\delta\sigma(t) = 0$  and add and subtract Eqs. (20b) and (20c) to obtain the following equations of motion

$$[\delta\ddot{x}_{+1}(t) + \delta\ddot{x}_{-1}(t)] + [\delta x_{+1}(t) + \delta x_{-1}(t)] = 0, \quad (24a)$$

$$[\delta\ddot{x}_{+1}(t) - \delta\ddot{x}_{-1}(t)] + [\delta x_{+1}(t) - \delta x_{-1}(t)] = \frac{1}{\sqrt{2\pi}} \frac{(c_0 - c_2)}{\sigma^3} [\delta x_{+1}(t) - \delta x_{-1}(t)] \quad (24b)$$

In terms of center of mass coordinate,  $\delta x_1(t) + \delta x_{-1}(t)$ , and relative coordinate,  $\delta x_1(t) - \delta x_{-1}(t)$ , Eq. (24a) corresponds to the center of mass motion oscillating with trap frequency  $\omega = 1$  satisfying Kohn's theorem and Eq. (24b) corresponds to frequency

$$\omega_{sd} = \sqrt{\left(1 - \sqrt{\frac{1}{2\pi}} \frac{(c_0 - c_2)}{\sigma^3}\right)} \quad (25)$$

of spin-dipole mode. For  $c_0 = 0.0119N$  and  $c_2 = 0.000424N$  with  $N = 4000$ , we get  $\omega_{sd} = 0.23$  which is very close to spin-dipole frequency 0.25 calculated from BdG analysis shown in Fig. 2. Eqs. (24a), (24b) also point out that in the presence of harmonic trap, center of mass and relative motions are decoupled.

#### IV. COLLECTIVE EXCITATIONS AT FINITE TEMPERATURE

We now analyze the excitation spectra of the SO-coupled  $^{23}\text{Na}$  spin-1 BEC with  $c_0 = 0.0119N$ ,  $c_2 = 0.000424N$ ,  $\gamma = 0.5$  at finite temperatures and consisting of (a)  $N = 2000$  and (b)  $N = 4000$ . The excitation spectrum is calculated by solving Eqs. (4a)-(4b) and (5) self-consistently with the non-condensate density computed from Eq. (6). As an example of static density profiles, the condensate and the non-condensate densities of the system with  $N = 4000$  are shown in Fig. 11 at  $T = 0.2T_c$  and  $T = 0.4T_c$ , where  $T_c = 40.56$  nK is the critical temperature for ideal spin-1 Bose gas in quasi-1D harmonic trap [62–64]. In Figs. 11 (a)-(b), we show the density profiles with  $H_{\text{SOC}} = \gamma p_x f_x$ , whereas in (c)-(d) the same with  $H'_{\text{SOC}} = \gamma p_x f_z$  are shown. With increasing temperature, the number of thermal atoms increases along with the spatial extent of the thermal cloud. This is accompanied by a corresponding decrease in the condensate density. The repulsive interaction between the condensate and non-condensate clouds results in a dip in the non-condensate density at the center of the trap and emergence of density peaks towards the edges of the trap as shown in Figs. 11(a)-(d).

In Fig. 12(a)-(b), we show the excitation spectra of non-zero modes as a function of temperature in the presence of SO coupling for  $N = 2000$  and  $N = 4000$ , respectively. With an increase in temperature the density and the spin modes show qualitatively distinct behavior. We observe that the frequencies of density modes decrease with an increase in temperature, whereas those of spin modes increase with the temperature. The behavior of density modes can be understood by the fact that at higher temperatures, the excitations are those of a condensate in an effective potential, and that the effective potential is weakened [65] by the presence of the static thermal cloud, thus lowering the harmonic potential and thereby decreasing the frequency. On the other hand, the increasing of spin modes' frequencies can be understood by the fact that at finite temperature, number of atoms in the condensates are decreasing, so by using an equivalent zero temperature condensate (EzC) [66] solution, we get qualitatively same behav-

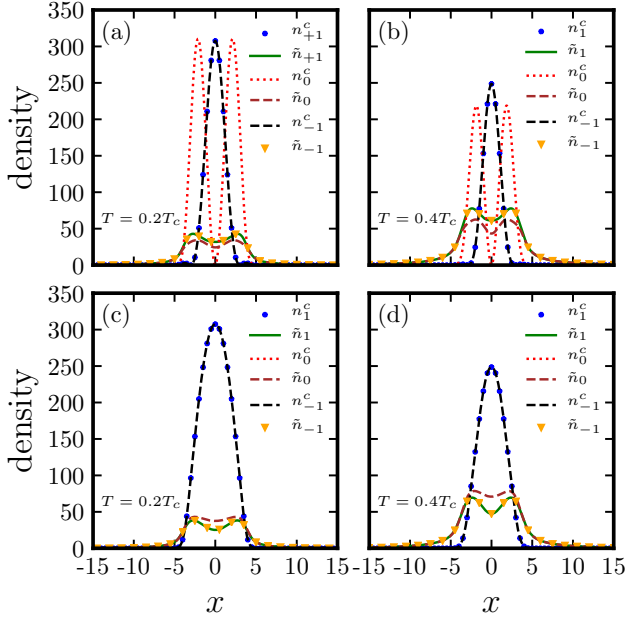


FIG. 11. Condensate densities,  $n_i^c(x)$ , and thermal densities,  $\tilde{n}_i(x)$ , for  $^{23}\text{Na}$  spin-1 BEC with  $c_0 = 0.00119N$ ,  $c_2 = 0.000424N$ ,  $N = 4000$ ,  $\gamma = 0.5$ , and  $H_{\text{soc}} = \gamma f_x p_x$  at (a)  $T = 0.2T_c$  and (b)  $T = 0.4T_c$ . The same for  $H'_{\text{soc}} = \gamma f_z p_x$  at  $T = 0.2T_c$  and  $T = 0.4T_c$  are shown, respectively, in (c) and (d).

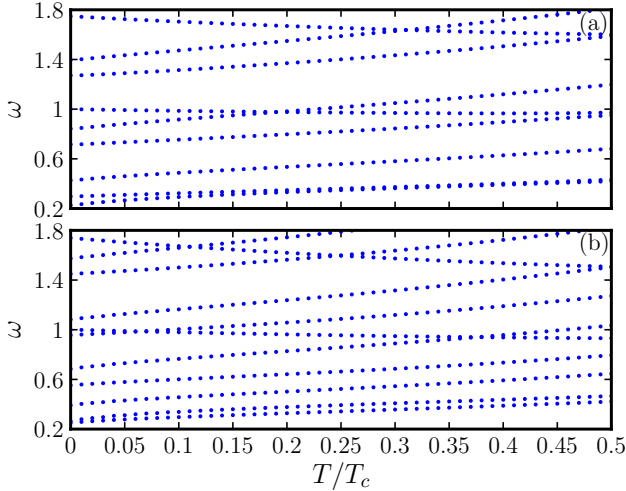


FIG. 12. (a) The excitation spectrum of  $^{23}\text{Na}$  spin-1 BEC at finite temperature with  $c_0 = 0.00119N$ ,  $c_2 = 0.000424N$ ,  $N = 2000$ , and  $\gamma = 0.5$ . The same for  $N = 4000$  is shown in (b).

ior for spin modes as shown in Figs. 12. It must be noted from Fig. 2 that for  $N \geq 2000$  the spin modes are much more sensitive to change in number of atoms in the condensate as compared to the density modes like breathing and dipole modes. The former decrease with an increase in number of atoms whereas the latter remain almost unchanged. The spin modes therefore increase with an increase of temperature as

the number of atoms in the condensate is decreasing. The density modes on other hand are more sensitive to change in the effective potential due to the thermal cloud. In order to further ascertain the role of thermal cloud on the density modes, we extend the variational analysis of Sec. III E to finite temperatures [67] for a density-breathing mode. We assume the thermal cloud as a static classical gas and write [67]

$$\tilde{n}_i = r(T) \exp[-V(x)/k_B T], \quad (26)$$

where  $r(T)$  is the normalization constant. The thermal-cloud density is normalized as  $\int \sum_i dx \tilde{n}_i(x) = N_T$ , where  $N_T$  is the number of atoms in thermal cloud. Energy with thermal cloud's contribution included can be written as  $E + E_T$ , where

$$E_T = [(c_0 + c_2)(\tilde{n}_{+1}|\phi_{+1}|^2 + \tilde{n}_{-1,-1}|\phi_{-1}|^2) + (c_0 - c_2)(\tilde{n}_{+1}|\phi_{-1}|^2 + \tilde{n}_{-1,-1}|\phi_{+1}|^2)], \quad (27)$$

and  $E$  is defined in Eq. (19). Replacing  $E$  by  $E + E_T$  in Lagrangian (18) and using the ansatz (17), the linearized equation of motion for the condensate width  $\sigma$  is

$$\ddot{\sigma}(t) + \left(1 + \frac{3}{\sigma^4} + \sqrt{\frac{2}{\pi}} \frac{c_0}{\sigma^3} - f(T)\right) \delta\sigma(t) = 0, \quad (28)$$

where  $f(T) = \sqrt{\frac{1}{2\pi}} c_0 N_T / (k_B T)^{3/2}$  and condensate width has been considered to be much smaller than the width of the thermal cloud. The frequency of the density-breathing mode from Eq. (28) is

$$\omega_b = \left[1 + \frac{3}{\sigma^4} + \sqrt{\frac{2}{\pi}} \frac{c_0}{\sigma^3} - f(T)\right]^{1/2}, \quad (29)$$

where  $f(T)$  in the square bracket results in the decrease in  $\omega_b$  as a function of temperature  $T$ .

## V. CONCLUSIONS

In this work, we have investigated the collective excitations of a quasi-1D interacting SO-coupled spin-1 BEC with antiferromagnetic spin-exchange interactions at zero and finite temperatures by employing the HFB-Popov approximation. In this approximation, the static properties of the system are very well described by GP equations which are coupled to BdG equations. Although as per the Popov approximation, we have neglected the anomalous average terms in the generalized GP equations and the BdG equations, we have included and illustrated the importance of the coherence terms between the thermal atoms of different components. The low lying modes of the interacting spin-1 BEC in the absence of SO coupling are characterized by the three Goldstone modes and doubly degenerate spin modes. With the introduction of an SO coupling, the degeneracy between the two spin modes is lifted where one of the modes increases with an increase in SO coupling strength while the other remains unchanged. We calculate the dispersion curves showing explicitly that the energy of

density excitations are always higher than the corresponding spin excitations, and moreover in the presence of SO coupling, dispersion has three distinct branches consistent with a breakdown in the degeneracy of the spin modes. To substantiate our theoretical prediction of the low-lying modes through physical observables useful for experiments, we have performed dynamical real-time simulations of the system by evolving the ground state in the presence of perturbations. We indeed find the dominant frequencies of oscillation in the center of mass and mean-square radius both in the spin and density channels are in excellent agreement with the Bogoliubov calculations. Considering a pseudo-spinor subsystem, we have also carried out a time-dependent variational analysis and demonstrated that the analytical and numerical results match quite well with each other. The collective excitations and equilibrium density profiles at non-zero temperatures are also presented. While

the energy of the density modes decreases with an increase in temperature, the energy of the spin modes increases. A natural extension of this work would be to compute systematically the phase diagram of the interacting SO-coupled spin-1 BEC and to study the dynamics of the collective excitations at finite temperatures.

### Acknowledgements

SG acknowledges the support of the Science and Engineering Research Board (SERB), Department of Science and Technology, Government of India under the projects ECR/2017/001436 and CRG/2021/002597.

- 
- [1] D. M. Stamper-Kurn, M. R. Andrews, A. P. Chikkatur, S. Inouye, H.-J. Miesner, J. Stenger, and W. Ketterle, *Phys. Rev. Lett.* **80**, 2027 (1998).
  - [2] M. D. Barrett, J. A. Sauer, and M. S. Chapman, *Phys. Rev. Lett.* **87**, 010404 (2001).
  - [3] M.-S. Chang, C. D. Hamley, M. D. Barrett, J. A. Sauer, K. M. Fortier, W. Zhang, L. You, and M. S. Chapman, *Phys. Rev. Lett.* **92**, 140403 (2004).
  - [4] T. Kuwamoto, K. Araki, T. Eno, and T. Hirano, *Phys. Rev. A* **69**, 063604 (2004).
  - [5] H. Schmaljohann, M. Erhard, J. Kronjäger, M. Kottke, S. van Staa, L. Cacciapuoti, J. J. Arlt, K. Bongs, and K. Sengstock, *Phys. Rev. Lett.* **92**, 040402 (2004).
  - [6] Y. Kawaguchi and M. Ueda, *Phys. Rep.* **520**, 253 (2012), spinor Bose–Einstein condensates.
  - [7] D. M. Stamper-Kurn and M. Ueda, *Rev. Mod. Phys.* **85**, 1191 (2013).
  - [8] Y.-J. Lin, K. Jiménez-García, and I. B. Spielman, *Nature (London)* **471**, 83 (2011).
  - [9] M. Z. Hasan and C. L. Kane, *Rev. Mod. Phys.* **82**, 3045 (2010).
  - [10] E. van der Bijl and R. A. Duine, *Phys. Rev. Lett.* **107**, 195302 (2011).
  - [11] H. Zhai, *Rep. Prog. Phys.* **78**, 026001 (2015).
  - [12] D. Campbell, R. Price, A. Putra, A. Valdés-Curiel, D. Trypogeorgos, and I. Spielman, *Nat. Commun.* **7**, 1 (2016).
  - [13] X. Luo, L. Wu, J. Chen, Q. Guan, K. Gao, Z.-F. Xu, L. You, and R. Wang, *Sci. Rep.* **6**, 1 (2016).
  - [14] C. Wang, C. Gao, C.-M. Jian, and H. Zhai, *Phys. Rev. Lett.* **105**, 160403 (2010).
  - [15] G. I. Martone, F. V. Pepe, P. Facchi, S. Pascazio, and S. Stringari, *Phys. Rev. Lett.* **117**, 125301 (2016).
  - [16] L. Chen, H. Pu, Z.-Q. Yu, and Y. Zhang, *Phys. Rev. A* **95**, 033616 (2017).
  - [17] B. A. Malomed, *Europhys. Lett.* **122**, 36001 (2018).
  - [18] K. Kasamatsu, M. Tsubota, and M. Ueda, *Int. J. Mod. Phys. B* **19**, 1835 (2005).
  - [19] C. J. Pethick and H. Smith, *Bose–Einstein Condensation in Dilute Gases* (Cambridge University Press, 2008).
  - [20] L. Pitaevskii and S. Stringari, *Bose–Einstein condensation and superfluidity*, Vol. 164 (Oxford University Press, 2016).
  - [21] M.-O. Mewes, M. R. Andrews, N. J. van Druten, D. M. Kurn, D. S. Durfee, C. G. Townsend, and W. Ketterle, *Phys. Rev. Lett.* **77**, 988 (1996).
  - [22] Y. Li, G. I. Martone, L. P. Pitaevskii, and S. Stringari, *Phys. Rev. Lett.* **110**, 235302 (2013).
  - [23] Z.-Q. Yu, *Phys. Rev. A* **93**, 033648 (2016).
  - [24] K. Sun, C. Qu, Y. Xu, Y. Zhang, and C. Zhang, *Phys. Rev. A* **93**, 023615 (2016).
  - [25] T. Ozawa, L. P. Pitaevskii, and S. Stringari, *Phys. Rev. A* **87**, 063610 (2013).
  - [26] M. A. Kamehchi, Y. Zhang, C. Hamner, T. Busch, and P. Engels, *Phys. Rev. A* **90**, 063624 (2014).
  - [27] S.-C. Ji, L. Zhang, X.-T. Xu, Z. Wu, Y. Deng, S. Chen, and J.-W. Pan, *Phys. Rev. Lett.* **114**, 105301 (2015).
  - [28] M. Tylutki, G. E. Astrakharchik, B. A. Malomed, and D. S. Petrov, *Phys. Rev. A* **101**, 051601 (2020).
  - [29] T. Isoshima, T. Ohmi, and K. Machida, *J. Phys. Soc. Jpn* **69**, 3864 (2000).
  - [30] W. Zhang, S. Yi, and L. You, *Phys. Rev. A* **70**, 043611 (2004).
  - [31] N. T. Phuc, Y. Kawaguchi, and M. Ueda, *Phys. Rev. A* **84**, 043645 (2011).
  - [32] Y. Kawaguchi, N. T. Phuc, and P. B. Blakie, *Phys. Rev. A* **85**, 053611 (2012).
  - [33] D. Jacob, L. Shao, V. Corre, T. Zibold, L. De Sarlo, E. Mimoun, J. Dalibard, and F. Gerbier, *Phys. Rev. A* **86**, 061601 (2012).
  - [34] J. Mur-Petit, M. Guilleumas, A. Polls, A. Sanpera, M. Lewenstein, K. Bongs, and K. Sengstock, *Phys. Rev. A* **73**, 013629 (2006).
  - [35] M. Moreno-Cardoner, J. Mur-Petit, M. Guilleumas, A. Polls, A. Sanpera, and M. Lewenstein, *Phys. Rev. Lett.* **99**, 020404 (2007).
  - [36] E. Witkowska, T. Świsłocki, and M. Matuszewski, *Phys. Rev. A* **90**, 033604 (2014).
  - [37] X.-L. Chen, X.-J. Liu, and H. Hu, *Phys. Rev. A* **96**, 013625 (2017).
  - [38] S.-C. Ji, J.-Y. Zhang, L. Zhang, Z.-D. Du, W. Zheng, Y.-J. Deng, H. Zhai, S. Chen, and J.-W. Pan, *Nat. Phys.* **10**, 314 (2014).
  - [39] Z.-Q. Yu, *Phys. Rev. A* **90**, 053608 (2014).
  - [40] T. Ozawa and G. Baym, *Phys. Rev. Lett.* **109**, 025301 (2012).
  - [41] E. Kawasaki and M. Holzmann, *Phys. Rev. A* **95**, 051601 (2017).
  - [42] S.-W. Su, I.-K. Liu, S.-C. Gou, R. Liao, O. Fialko, and J. Brand, *Phys. Rev. A* **95**, 053629 (2017).

- [43] R. M. Wilson, S. Ronen, and J. L. Bohn, *Phys. Rev. Lett.* **104**, 094501 (2010).
- [44] T.-L. Ho, *Phys. Rev. Lett.* **81**, 742 (1998).
- [45] T. Ohmi and K. Machida, *J. Phy. Soc. Jpn* **67**, 1822 (1998).
- [46] A. Griffin, *Phys. Rev. B* **53**, 9341 (1996).
- [47] A. Roy, S. Gautam, and D. Angom, *Phys. Rev. A* **89**, 013617 (2014).
- [48] A. Roy and D. Angom, *Phys. Rev. A* **90**, 023612 (2014).
- [49] N. M. Hugenholtz and D. Pines, *Phys. Rev.* **116**, 489 (1959).
- [50] P. Kaur, A. Roy, and S. Gautam, *Comput. Phys. Commun.* **259**, 107671 (2021).
- [51] P. Banger, P. Kaur, and S. Gautam, *Int. J. Mod. Phys. C* , 2250046 (2021).
- [52] Y. Gao and Y. Cai, *J. Comput. Phys.* **403**, 109058 (2020).
- [53] E. Serrano-Ensástiga and F. Mireles, *Phys. Rev. A* **104**, 063308 (2021).
- [54] C. Ticknor, *Phys. Rev. A* **89**, 053601 (2014).
- [55] S. Pal, A. Roy, and D. Angom, *J. Phys. B: At. Mol. Opt. Phys.* **51**, 085302 (2018).
- [56] S. Knoop, T. Schuster, R. Scelle, A. Trautmann, J. Appmeier, M. K. Oberthaler, E. Tiesinga, and E. Tiemann, *Phys. Rev. A* **83**, 042704 (2011).
- [57] H. Watanabe and H. Murayama, *Phys. Rev. Lett.* **108**, 251602 (2012).
- [58] J. F. Dobson, *Phys. Rev. Lett.* **73**, 2244 (1994).
- [59] T. Bienaimé, E. Fava, G. Colzi, C. Mordini, S. Serafini, C. Qu, S. Stringari, G. Lamporesi, and G. Ferrari, *Phys. Rev. A* **94**, 063652 (2016).
- [60] V. M. Pérez-García, H. Michinel, J. I. Cirac, M. Lewenstein, and P. Zoller, *Phys. Rev. Lett.* **77**, 5320 (1996).
- [61] V. M. Pérez-García, H. Michinel, J. I. Cirac, M. Lewenstein, and P. Zoller, *Phys. Rev. A* **56**, 1424 (1997).
- [62] W. Ketterle and N. J. van Druten, *Phys. Rev. A* **54**, 656 (1996).
- [63] Kao, Y.-M. and Jiang, T. F., *Eur. Phys. J. D* **40**, 263 (2006).
- [64] W.-J. Huang, S.-C. Gou, and Y.-C. Tsai, *Phys. Rev. A* **65**, 063610 (2002).
- [65] C. Gies, B. P. van Zyl, S. A. Morgan, and D. A. W. Hutchinson, *Phys. Rev. A* **69**, 023616 (2004).
- [66] R. J. Dodd, M. Edwards, C. W. Clark, and K. Burnett, *Phys. Rev. A* **57**, R32 (1998).
- [67] H. Shi and W.-M. Zheng, *Phys. Rev. A* **59**, 1562 (1999).